

# The Cosmic Microwave Background for a Nearly Flat Compact Hyperbolic Universe

R. Aurich and F. Steiner

*Abteilung Theoretische Physik, Universität Ulm  
Albert-Einstein-Allee 11, D-89069 Ulm  
Federal Republic of Germany*

Accepted ???, Received ???; in original form 13 December 2018

## ABSTRACT

The fluctuations of the cosmic microwave background (CMB) are investigated for a hyperbolic universe with finite volume. Four-component models with radiation, matter, vacuum energy, and an extra spatially constant dark energy  $X$ -component are considered. The general solution of the Friedmann equation for the cosmic scale factor  $a(\eta)$  is given for the four-component models in terms of the Weierstrass  $\mathcal{P}$ -function. The lower part of the angular power spectra  $C_l$  of the CMB anisotropy is computed for nearly flat models with  $\Omega_{\text{tot}} \leq 0.95$ . It is shown that the particular compact fundamental cell, which is considered in this paper, leads to a suppression in  $C_l$  for  $l \lesssim 10$  and  $\Omega_{\text{tot}} \lesssim 0.9$ .

**Key words:** cosmology:theory – cosmic microwave background – large-scale structure of universe – topology – dark matter – cosmological constant – quintessence

## 1 INTRODUCTION

The two crucial properties of the universe at large scales are its curvature and its topology. Both properties are encoded in the cosmic microwave background (CMB), see e. g. (Hu and White, 1996; Cornish et al., 1998; Kamionkowski and Buchalter, 2000), which is measured with ever increasing resolution. The detection of the first acoustic peak in the CMB angular power spectrum  $C_l$  (Knox and Page, 2000) provides evidence for a flat, or nearly flat, cold dark matter universe with a non-vanishing cosmological constant and/or an extra exotic energy component. The recent Boomerang (de Bernardis et al., 2000) and MAXIMA-1 (Hanany et al., 2000) measurements yield evidence even for the second acoustic peak which is, however, less pronounced than expected by standard CMB models. These CMB scenarios are based on isentropic initial perturbations in a universe composed of radiation, baryonic matter according to the Big Bang nucleosynthesis, cold dark matter, and a non-vanishing cosmological constant. Possible explanations for the low second peak and the surprisingly large scale of the first peak are discussed in (White et al., 2000; Tegmark and Zaldarriaga, 2000; Cornish, 2000; Weinberg, 2000b). The constraints obtained from the MAXIMA-1 experiment are  $\Omega_{\text{tot}} = 0.90 \pm 0.15$ ,  $\Omega_{\text{bar}} h_0^2 = 0.025 \pm 0.010$ ,  $\Omega_{\text{cdm}} h_0^2 = 0.13 \pm 0.10$ , and a spectral index  $n = 0.99 \pm 0.09$  at 95% confidence level (Balbi et al., 2000). Here  $\Omega_{\text{cdm}}$  and  $\Omega_{\text{bar}}$  denote the ratio of the cold dark matter (cdm) and baryonic (bar) energy densities, respectively, to the critical energy density.

The standard models describe the structure of the acoustic peaks, but fail to match with the low quadrupole moment  $C_2$  of the COBE experiment (Tegmark and Hamilton, 1997). This can

be interpreted as a hint for a non-trivial topology of our universe. The standard models suppose a trivial topology implying a universe with infinite volume for negative and zero curvature. Models with a non-trivial topology lead to a finite volume and to a suppression in the angular power spectrum  $C_l$  for low multipoles. This motivates the study of non-trivial topologies (Lachièze-Rey and Luminet, 1995) which leads to multiple images of a single source called topological lensing (Uzan et al., 2000), and the just mentioned suppression in the large scale CMB anisotropy on which we concentrate in this paper. For flat models the topological length scale is constrained to be significantly larger than half the diameter of the observable universe (Levin et al., 1998) which renders these models unattractive. (See, however, (Roukema, 2000).) Thus in the following we discuss models with negative curvature.

The computation of the CMB anisotropy for compact hyperbolic universes can be carried out in two different ways. On the one hand one can compute the fluctuations by using the so-called method of images which requires the group elements which define the fundamental cell of the considered non-trivial topology (Bond et al., 1998; Bond et al., 2000a; Bond et al., 2000b). On the other hand one can use a method which requires the eigenmodes of the fundamental cell with respect to the Laplace-Beltrami operator of the considered space. With the latter method the CMB anisotropy is computed for hyperbolic universes with a vanishing cosmological constant  $\Lambda$  for a compact orbifold (Aurich, 1999) and several compact manifolds (Inoue et al., 1999; Cornish and Spergel, 2000).

Our main aim in this paper is to incorporate a non-vanishing cosmological constant  $\Lambda$  and, in addition, an extra smooth dark energy component  $\varepsilon_x$  (Turner and White, 1997) in the anisotropy calculations as suggested by current observations, where we concen-

arXiv:astro-ph/0007264v2 6 Oct 2000

trate on the lower part of the angular power spectrum  $C_l$ , which is affected by the non-trivial topology. Recent investigations, in particular of the luminosity-redshift surveys of Type Ia supernovae (Riess et al., 1998; Perlmutter et al., 1999), strongly indicate that current observations require apart from a matter density component  $\Omega_{\text{mat}} = \Omega_{\text{cdm}} + \Omega_{\text{bar}} \simeq 0.3 \pm 0.1$  an additional unclustered, dark energy component of 60% of the total energy density of the universe with negative pressure (Wang et al., 2000; Hu et al., 2000) corresponding to an accelerated expansion. In the following we will assume that the new component is a mixture of vacuum energy,  $\Omega_{\text{vac}}$ , or cosmological constant  $\Lambda$ , and a smooth dark energy component  $\Omega_x$ . Whereas a cosmological constant  $\Lambda > 0$  corresponds to a constant homogeneous energy component  $\epsilon_{\text{vac}} > 0$  with negative pressure and equation of state  $w_{\text{vac}} = -1$ , the extra dark energy component  $X$  considered by us consists of a dynamical, time-dependent energy density  $\epsilon_x > 0$  with negative pressure and equation of state  $w_x = -\frac{2}{3}$ . (Here  $w$  denotes the ratio of pressure to energy density.) The  $X$ -component is similar to a particular version of quintessence which is generated by a slowly evolving scalar field with an exponential or inverse power law potential and  $-1 < w_{\text{quint}} \leq 0$  (Ratra and Peebles, 1988; Peebles and Ratra, 1988; Wetterich, 1988a; Wetterich, 1988b; Caldwell et al., 1998). The quintessence models and the more recent “tracker field” models (Zlatev et al., 1999) have been introduced to solve the two cosmological constant problems (Weinberg, 2000a): i) why is  $\epsilon_{\text{vac}}$  so small, ii) why is  $\epsilon_{\text{vac}}$  not only small, but also of the same magnitude as the present mass of the universe? (See also (Armendariz-Picon et al., 2000a; Armendariz-Picon et al., 2000b) for the concept of “k-essence” and (Weinberg, 2000a) for an anthropic explanation.) While at present there is no direct evidence for a scalar field, let alone for a particular form of the potential, observations are consistent with an  $X$ -component if  $w_x = -0.65 \pm 0.07$  (assuming flat models) (Wang et al., 2000). However, since the concept of a scalar quintessence field is a purely classical phenomenological one, we expect the quantum mechanics of such a theory to be plagued with the usual problem of nonrenormalizability (Ratra and Peebles, 1988; Peebles and Ratra, 1988). We therefore adopt in this paper the point of view of an effective quintessence model, where we do not start from a given potential for the scalar field, but rather give the redshift behavior  $\epsilon_x \sim a^{-1}$  and thus the equation of state  $w_x = -\frac{2}{3}$ , which is consistent with the above cited experimental bounds ( $a$  is the cosmic scale factor, see the next section). Furthermore, we will assume that the  $X$ -component is spatially constant which can be understood as follows (Ratra and Peebles, 1988; Peebles and Ratra, 1988). In linear perturbation theory spatial gradients in the scalar field act like particles with very low mass that cannot bind to a nonrelativistic gravitational potential well that is much smaller than the Hubble length  $H^{-1}$ . Thus dynamical studies of groups and clusters of galaxies with size  $\ll H^{-1}$  cannot detect concentrations in  $\epsilon_x$ , and thus  $\epsilon_x$  can be assumed to be spatially constant. This is confirmed by recent determinations of  $\Omega_{\text{mat}}$  obtained from relative velocities of galaxies yielding results in the range  $0.2 \lesssim \Omega_{\text{mat}} \lesssim 0.4$  (Juszkiewicz et al., 2000; Willick, 2000). Since these measurements are sensitive to a spatially inhomogeneous dark energy component (Lahav et al., 1991), we have to assume the dark energy component, required by CMB measurements, to be smooth. Therefore, we assume below an  $X$ -component being spatially homogeneous like the vacuum energy and  $\Omega_{\text{mat}} = 0.3$ . (For further arguments concerning the smoothness assumption, see (Turner and White, 1997; White, 1998).)

The fundamental cell which we consider in this paper is the same pentahedron as considered in (Aurich, 1999) with the same Dirichlet eigenmode spectrum. (For more details, see also (Aurich

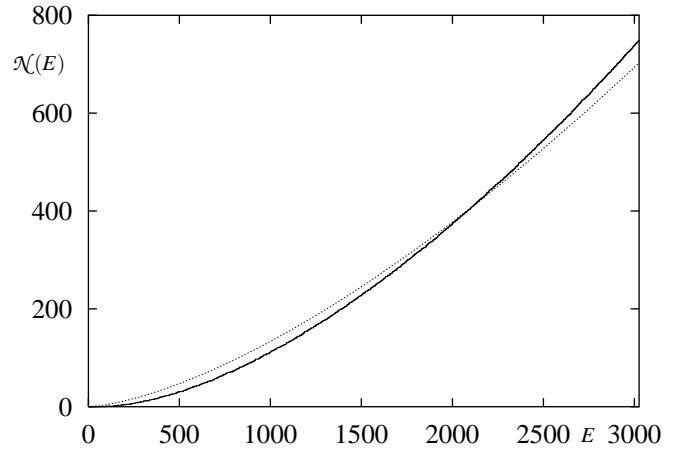


**Figure 1.** The number  $\mathcal{N}(E)$  of eigenvalues below  $E$  is shown together with Weyl’s law for the tetrahedral fundamental cell with Dirichlet boundary conditions (dashed curve, not visible) and Weyl’s law for a manifold with volume 0.25 (dotted curve),  $R = 1$ .

and Marklof, 1996.) One is interested in fundamental cells with volumes as small as possible for several reasons, e. g. the creation probability of the universe increases dramatically with decreasing volume (Atkatz and Pagels, 1982) and, furthermore, to obtain an appreciable effect in the CMB anisotropy. Unfortunately, the smallest hyperbolic manifold  $\mathcal{M}$  is unknown. The smallest one known has a volume  $\text{vol}(\mathcal{M}) = 0.94272\dots R^3$ , which is far above the lower bound  $\text{vol}(\mathcal{M}) > 0.16668\dots R^3$  (Gabai et al., 1996). Here  $R$  denotes the curvature radius of the universal covering space.

Concerning the impact on the CMB anisotropy the main difference with respect to infinite-volume models arises from the discrete eigenvalue spectrum  $\{E_n\}$  which compact manifolds possess in contrast to the continuous spectrum of the infinite volume models. The volume of the manifold has an important influence on the CMB anisotropy because it determines the magnitude of the lowest eigenmode and the number of eigenmodes below a given value  $E$ . For a manifold  $\mathcal{M}$ , the number  $\mathcal{N}(E)$  of eigenvalues below  $E$  is asymptotically given by Weyl’s law ( $R = 1$ )

$$\mathcal{N}(E) \sim \frac{\text{vol}(\mathcal{M})}{6\pi^2} k^3 \quad \text{with} \quad k := \sqrt{E-1} \quad .$$

The first lowest eigenmodes determine the largest scales of the CMB anisotropies. The smaller the volume the stronger is the suppression of the first multipoles in the angular power spectrum  $C_l$ .

The considered pentahedron has a volume  $\text{vol}(\mathcal{M}) \simeq 0.7173068R^3$ . Since only one of two symmetry classes is taken into account, the following computations correspond to a hyperbolic manifold with  $\text{vol}(\mathcal{M}) \simeq 0.3586534R^3$ . However, a volume comparison is complicated by the fact that Weyl’s law has additional terms for orbifolds in comparison to manifolds, in particular the surface term (Aurich and Marklof, 1996) being absent in the case of manifolds. The additional surface term leads to a suppression of  $\mathcal{N}(E)$  in comparison with manifolds as shown in figure 1 for  $E < 3026$ . The figure demonstrates that the considered orbifold mimics a manifold with effective volume  $\simeq 0.25R^3$ . The statistical properties of the eigenmodes are expected to be of the same random nature as observed in quantum chaos (Aurich and Steiner, 1993; Inoue, 1999).

## 2 THE BACKGROUND MODEL

The standard cosmological model based on the Friedmann-Le-maître-Robertson-Walker metric ( $c = 1$ )

$$ds^2 = a^2(\eta) \left\{ d\eta^2 - \gamma_{ij} dx^i dx^j \right\}$$

is governed for negative curvature ( $K = -1$ ) by the Friedmann equation

$$a'^2 - a^2 = \frac{8\pi G}{3} T_0^0 a^4, \quad ,$$

where  $a(\eta)$  is the cosmic scale factor and  $\eta$  the conformal time. The prime denotes differentiation with respect to  $\eta$ . The energy-momentum tensor for an ideal fluid is given by

$$T_\nu^\mu = (\varepsilon + p)u^\mu u_\nu - p\delta_\nu^\mu, \quad ,$$

where  $u^\mu$  is the four-velocity of the fluid, and  $\varepsilon = \varepsilon(\eta)$  denotes the energy density and  $p = p(\eta)$  the pressure. In the following we consider multi-component models containing a matter-energy density  $\varepsilon_{\text{mat}}$ , a radiation density  $\varepsilon_{\text{rad}}$  as well as a non-vanishing cosmological constant  $\Lambda = 8\pi G\varepsilon_{\text{vac}}$  and a spatially constant  $X$ -component  $\varepsilon_x$  with an equation of state  $p_x = -\frac{2}{3}\varepsilon_x$ . Then the 00-component of the energy-momentum tensor is given in comoving coordinates by

$$T_0^0 = \sum_{\substack{k=0 \\ k \neq 2}}^4 \varepsilon_{k,0} \left( \frac{a_0}{a} \right)^k, \quad ,$$

expressed in terms of the current radiation density  $\varepsilon_{4,0} = \varepsilon_{\text{rad},0}$ , the current matter density  $\varepsilon_{3,0} = \varepsilon_{\text{mat},0}$ , the current  $X$ -component energy density  $\varepsilon_{1,0} = \varepsilon_{x,0}$  and a vacuum energy density  $\varepsilon_{0,0} = \varepsilon_{\text{vac}}$ . Here  $a_0 := a(\eta_0)$  is the scale factor of the present epoch. The present conformal time  $\eta_0$  is implicitly given by

$$a(\eta_0) = \frac{1}{H_0 \sqrt{1 - \Omega_{\text{tot}}}}, \quad \Omega_{\text{tot}} = \Omega_{\text{rad}} + \Omega_{\text{mat}} + \Omega_x + \Omega_{\text{vac}}, \quad ,$$

where  $H_0 = h_0 100 \text{ km s}^{-1} \text{ Mpc}^{-1}$  denotes Hubble's constant and  $\Omega_k := \varepsilon_{k,0}/\varepsilon_{\text{crit}}$  with  $\varepsilon_{\text{crit}} = 3H_0^2/(8\pi G)$ . With

$$\Omega_2 := \Omega_{\text{curv}} := -\frac{K}{(a_0 H_0)^2} = \frac{1}{(a_0 H_0)^2} = 1 - \Omega_{\text{tot}} > 0$$

the Friedmann equation reads

$$a'(\eta) = H_0 \sqrt{\sum_{k=0}^4 \Omega_k a_0^k a^{4-k}}. \quad (1)$$

This gives the infinitely far future  $\eta_\infty$  as

$$\eta_\infty = \sqrt{1 - \Omega_{\text{tot}}} \int_0^\infty \frac{dx}{\sqrt{\sum_{k=0}^4 \Omega_k x^k}}, \quad (2)$$

which yields  $\eta_\infty < \infty$  for a large class of models, see below. Notice that the various components redshift like  $a^{-k}$  with an associated equation of state  $w_k := p_k/\varepsilon_k = (k-3)/3$ . The current value of the deceleration parameter is given by  $q_0 = \Omega_{\text{rad}} + \frac{1}{2}\Omega_{\text{mat}} - \frac{1}{2}\Omega_x - \Omega_{\text{vac}}$ .

Let us define the following quantities

$$A := \frac{1}{2}\Omega_{\text{mat}}H_0^2 a_0^3 = \frac{2a_{\text{eq}}}{\eta^2}, \quad ,$$

$$B := \frac{1}{4}\Omega_x H_0^2 a_0, \quad ,$$

$$C := \frac{1}{12}A^2 \eta^2 \Lambda$$

with

$$\hat{\eta} := \frac{2\sqrt{\Omega_{\text{rad}}}}{H_0 a_0 \Omega_{\text{mat}}} \simeq (1 + \sqrt{2}) \eta_{\text{eq}}, \quad ,$$

where the subscript ‘‘eq’’ marks the epoch of matter-radiation equality, and  $a_{\text{eq}} := a(\eta_{\text{eq}}) = a_0(\Omega_{\text{rad}}/\Omega_{\text{mat}})$ . With the initial conditions  $a(0) = 0$  and  $a'(0) > 0$ , equation (1) has the unique solution

$$a(\eta) = \frac{A}{2} \frac{\mathcal{P}(\eta) - \frac{1}{12} - \hat{\eta} \mathcal{P}'(\eta) + AB\hat{\eta}^2}{(\mathcal{P}(\eta) - \frac{1}{12})^2 - C}. \quad (3)$$

Here  $\mathcal{P}(\eta)$  denotes the Weierstrass  $\mathcal{P}$ -function which can numerically be evaluated very efficiently by

$$\mathcal{P}(\eta) = \mathcal{P}(\eta; g_2, g_3) = \frac{1}{\eta^2} + \sum_{k=2}^{\infty} c_k \eta^{2k-2} \quad (4)$$

with

$$c_2 := \frac{g_2}{20}, \quad c_3 := \frac{g_3}{28}$$

and (Abramowitz and Stegun, 1965)

$$c_k = \frac{3}{(2k+1)(k-3)} \sum_{m=2}^{k-2} c_m c_{k-m} \quad \text{for } k \geq 4. \quad ,$$

The so-called invariants  $g_2$  and  $g_3$  are determined by the cosmological parameters

$$\begin{aligned} g_2 &= \frac{1}{12} + 4C - 2AB \\ g_3 &= -\frac{1}{216} + \frac{8C - A^2\Lambda}{12} + \frac{AB}{6} - A^2 B^2 \hat{\eta}^2. \end{aligned}$$

For cosmologically plausible parameter choices the series (4) needs only to be evaluated by taking into account the first twenty terms and thus the explicit solution (3) is much more efficient than the usual integration of the Friedmann equation.

Expanding (3) in a series at  $\eta = 0$  gives the scale factor at early times

$$\begin{aligned} a(\eta) &= A \left\{ \hat{\eta} \eta + \frac{\eta^2}{2} + \hat{\eta} \frac{\eta^3}{3!} + \left( 1 + 12AB\hat{\eta}^2 \right) \frac{\eta^4}{4!} \right. \\ &\quad \left. + \hat{\eta} (1 + 36AB + 48C) \frac{\eta^5}{5!} + O(\eta^6) \right\}. \end{aligned}$$

This expansion shows that the  $X$ -component term  $B$  influences the scale factor one power in  $\eta$  lower than the cosmological constant term  $C$ .

In the case  $\Lambda > 0$  and/or  $B > 0$  the conformal time  $\eta$  is restricted to  $0 \leq \eta < \eta_\infty < \infty$ , where  $\eta_\infty$ , defined in (2), is obtained from the implicit relation

$$\mathcal{P}(\eta_\infty; g_2, g_3) = \frac{1}{12} + \sqrt{C}. \quad ,$$

In the case  $\Lambda > 0$  the scale factor  $a(\eta)$  has a simple pole at  $\eta = \eta_\infty$  with residue  $-\sqrt{3/\Lambda}$ , i.e.

$$a(\eta) = \frac{\sqrt{3/\Lambda}}{\eta_\infty - \eta} - \frac{3}{\Lambda} B + O(\eta - \eta_\infty), \quad ,$$

which leads to an exponential expansion of the universe with scale factor  $R(t) = a(\eta(t)) = O(\exp(\sqrt{\Lambda/3}t))$  for cosmic time  $t \rightarrow \infty$ .

For  $\Lambda = 0$  and  $\Omega_x > 0$  one has at  $\eta = \eta_\infty$  a double pole, i.e.

$$a(\eta) = \frac{1/B}{(\eta - \eta_\infty)^2} - \frac{1}{12B} + O((\eta - \eta_\infty)^2), \quad ,$$

$\Omega_x$	$\Omega_{\text{vac}}$	$a_0$ [cm]	$t_0$ [Gyr]	$\eta_{\text{eq}}$	$\eta_{\text{SLS}}$	$\eta_0$	$\eta_\infty$	$N_{\text{Pentahedron}}$
0.00	0.00	15.797E+27	11.30	0.016	0.057	2.381	$\infty$	208
0.10	0.00	17.063E+27	11.46	0.015	0.053	2.231	5.364	151
0.20	0.00	18.692E+27	11.62	0.014	0.048	2.062	4.444	105
0.30	0.00	20.899E+27	11.80	0.012	0.043	1.868	3.765	68
0.40	0.00	24.132E+27	11.98	0.011	0.037	1.639	3.146	39
0.50	0.00	29.557E+27	12.18	0.009	0.030	1.357	2.505	19
0.60	0.00	41.805E+27	12.39	0.006	0.022	0.974	1.739	6
0.00	0.10	17.063E+27	11.53	0.015	0.053	2.240	3.780	154
0.10	0.10	18.692E+27	11.70	0.014	0.048	2.070	3.424	107
0.20	0.10	20.899E+27	11.88	0.012	0.043	1.876	3.047	69
0.30	0.10	24.132E+27	12.08	0.011	0.037	1.647	2.630	40
0.40	0.10	29.557E+27	12.28	0.009	0.030	1.364	2.144	19
0.50	0.10	41.805E+27	12.49	0.006	0.022	0.979	1.516	6
0.00	0.20	18.692E+27	11.79	0.014	0.048	2.079	3.253	109
0.10	0.20	20.899E+27	11.97	0.012	0.043	1.885	2.909	70
0.20	0.20	24.132E+27	12.17	0.011	0.037	1.655	2.521	41
0.30	0.20	29.557E+27	12.38	0.009	0.030	1.371	2.063	20
0.40	0.20	41.805E+27	12.60	0.006	0.022	0.984	1.463	6
0.00	0.30	20.899E+27	12.07	0.012	0.043	1.893	2.830	72
0.10	0.30	24.132E+27	12.27	0.011	0.037	1.663	2.458	42
0.20	0.30	29.557E+27	12.48	0.009	0.030	1.378	2.015	20
0.30	0.30	41.805E+27	12.71	0.006	0.022	0.989	1.432	6
0.00	0.40	24.132E+27	12.37	0.011	0.037	1.671	2.416	43
0.10	0.40	29.557E+27	12.59	0.009	0.030	1.385	1.983	20
0.20	0.40	41.805E+27	12.82	0.006	0.022	0.995	1.411	6
0.00	0.50	29.557E+27	12.70	0.009	0.030	1.392	1.960	21
0.10	0.50	41.805E+27	12.94	0.006	0.022	1.000	1.396	6
0.00	0.60	41.805E+27	13.06	0.006	0.022	1.006	1.385	6

**Table 1.** The present value of the scale factor  $a_0$  and the present age of the universe  $t_0$  as well as several important conformal times, i. e.  $\eta_{\text{eq}}$ , the time of recombination  $\eta_{\text{SLS}}$  at redshift  $z = 1200$ ,  $\eta_0$  and  $\eta_\infty$ , are given for  $\Omega_{\text{mat}} = 0.3$  and  $h_0 = 0.7$  and different combinations of  $\Omega_x$  and  $\Omega_{\text{vac}}$ . The number  $N_{\text{Pentahedron}}$  of pentahedrons within the surface of last scattering is also presented.

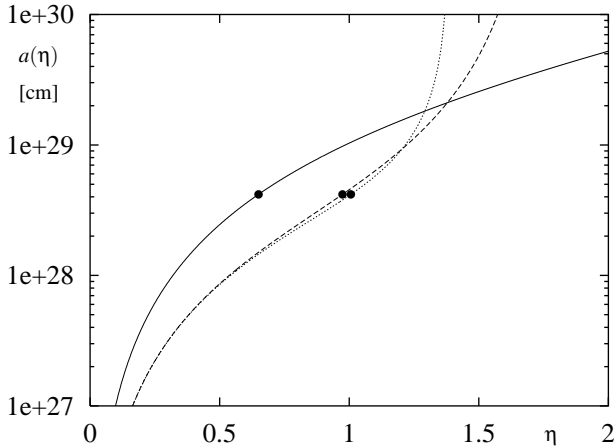


**Figure 2.** The scale factor is shown for nearly flat models with  $\Omega_{\text{tot}} = 0.9$  and  $h_0 = 0.7$ . The full curve corresponds to  $\Omega_{\text{mat}} = 0.9$ ,  $\Omega_x = \Omega_{\text{vac}} = 0.0$ , the dashed curve to  $\Omega_{\text{mat}} = 0.3$ ,  $\Omega_x = 0.6$  and  $\Omega_{\text{vac}} = 0.0$ , and the dotted curve to  $\Omega_{\text{mat}} = 0.3$ ,  $\Omega_x = 0.0$  and  $\Omega_{\text{vac}} = 0.6$ . The last model has the smallest  $\eta_\infty$ . The present scale factor  $a_0$  is indicated by a dot.

leading to  $R(t) = Bt^2 + \dots$  for  $t \rightarrow \infty$ , which follows from the exact

formula

$$t = -\frac{1}{12B}\eta(t) + \frac{1}{B}\zeta(\eta_\infty - \eta(t)) - \frac{1}{B}\zeta(\eta_\infty) \quad ,$$

where  $\zeta(\eta) := \zeta(\eta; g_2, g_3)$  denotes the Weierstrass zeta function. In this special case formula (3) reduces to  $(\mathcal{P}(\eta_\infty) = \frac{1}{12})$

$$a(\eta) = \frac{1}{B}\mathcal{P}(\eta - \eta_\infty) - \frac{1}{12B} \quad \text{with} \quad 0 \leq \eta < \eta_\infty \quad .$$

Finally, if both the cosmological constant and the  $X$ -component vanish,  $B = C = 0$ , the invariants simplify to  $g_2 = \frac{1}{12}$  and  $g_3 = -\frac{1}{216}$ , and the  $\mathcal{P}$ -function can be expressed in terms of an elementary function (Abramowitz and Stegun, 1965)

$$\mathcal{P}\left(\eta; \frac{1}{12}, -\frac{1}{216}\right) = \frac{1}{12} + \frac{1}{4\sinh^2 \frac{\eta}{2}} \quad ,$$

which, with (3), leads to  $a(\eta) = A(\hat{\eta} \sinh \eta + \cosh \eta - 1)$ , which is the well-known expression for the scale factor of a two-component model consisting of radiation and matter only. This leads to  $R(t) = t + A \ln t + O(1)$  for  $t \rightarrow \infty$ .

As an illustration we show in figure 2 the cosmic scale factor  $a(\eta)$  for three different, nearly flat models ( $\Omega_{\text{tot}} = 0.9$ ). The full curve corresponds to a two-component model consisting of radiation and matter ( $\Omega_{\text{mat}} = 0.9$ ) only. For this model  $\eta_\infty = \infty$  holds. The dashed curve represents a three-component model consisting of radiation, matter and an  $X$ -component ( $\Omega_x = 0.6$ ). The approach

to the double pole at  $\eta_\infty = 1.739$  is clearly visible. The dotted curve shows  $a(\eta)$  for a three-component model consisting of radiation, matter and vacuum energy ( $\Omega_{\text{vac}} = 0.6$ ). One observes a steep rise to the pole at  $\eta_\infty = 1.385$ . In addition we have indicated the present scale factor  $a_0$  by a dot.

In table 1 the scale factor  $a_0$  and the present age of the universe  $t_0$  as well as several cosmologically important times, i. e.  $\eta_{\text{eq}}$ ,  $\eta_{\text{SLS}}$ ,  $\eta_0$  and  $\eta_\infty$ , are given for several combinations of  $\Omega_k$ . The present age of the universe  $t_0$  is very close to the limit given by globular cluster ages  $13.5 \pm 2.0$  Gyr (Jimenez, 1999; Primack, 2000). White dwarf cooling rates lead to an age of our galaxy of  $9.3 \pm 2.0$  Gyr (Winget et al., 1987) or  $8.0 \pm 1.5$  Gyr (Leggett et al., 1998). For a smaller Hubble constant, e. g.  $h_0 = 0.6$ , the age  $t_0$  obtains larger values with  $13.18 \text{ Gyr} \leq t_0 \leq 15.24 \text{ Gyr}$ .

### 3 THE CMB ANISOTROPY

In the following we consider only scalar perturbations and their influence on the CMB. Furthermore, we assume that the vacuum energy  $\epsilon_{\text{vac}}$  and the other dark energy component  $\epsilon_x$  are spatially constant. The metric with scalar perturbations is written in the conformal-Newtonian gauge in terms of scalar functions  $\Phi$  and  $\Psi$  as

$$ds^2 = a^2(\eta) \left\{ (1 + 2\Phi)d\eta^2 - (1 - 2\Psi)\gamma_{ij}dx^i dx^j \right\} ,$$

where  $\Phi = \Psi$  for a diagonal  $T_{\mu\nu}$ . Assuming negligible entropy perturbations  $\delta S = 0$ , the evolution of the metric perturbation  $\Phi$  gives in first-order perturbation theory in the conformal-Newtonian gauge (Mukhanov et al., 1992)

$$\Phi'' + 3\hat{H}(1 + c_s^2)\Phi' - c_s^2\Delta\Phi + \{2\hat{H}' + (1 + 3c_s^2)(\hat{H}^2 + 1)\}\Phi = 0 ,$$

where  $\hat{H} := d'/a$  and  $\Delta$  denotes the Laplace-Beltrami operator. The quantity  $c_s^2$  can be interpreted as the sound velocity and is given by

$$c_s^2 = \frac{1}{3 + \frac{9}{4}\epsilon_{\text{mat}}/\epsilon_{\text{rad}}} .$$

Here it is assumed that the vacuum energy  $\epsilon_{\text{vac}}$  and the other dark energy component  $\epsilon_x$  are spatially constant.

Specifying  $\Phi$  at  $\eta = 0$  such that it corresponds to a scale-invariant (Harrison-Zel'dovich) spectrum, allows the computation of the time-evolution of the metric perturbation  $\Phi$ . This in turn gives the input to the Sachs-Wolfe formula (Sachs and Wolfe, 1967) which reads for isentropic initial conditions

$$\frac{\delta T}{T} = 2\Phi(\eta_{\text{SLS}}, \vec{x}(\eta_{\text{SLS}})) - \frac{3}{2}\Phi(0, \vec{x}(0)) + 2 \int_{\vec{x}(\eta_{\text{SLS}})}^{\vec{x}(\eta_0)} d\eta \frac{\partial\Phi(\eta, \vec{x}(\eta))}{\partial\eta} , \quad (5)$$

from which one obtains the desired temperature fluctuations  $\delta T$  of the CMB. The conformal time at recombination, which defines the surface of last scattering, is denoted by  $\eta_{\text{SLS}}$ . For  $\eta_{\text{SLS}} \gg \eta_{\text{eq}}$  the first two terms on the right-hand side are approximately

$$2\Phi(\eta_{\text{SLS}}, \vec{x}(\eta_{\text{SLS}})) - \frac{3}{2}\Phi(0, \vec{x}(0)) \simeq \frac{1}{3}\Phi(\eta_{\text{SLS}}, \vec{x}(\eta_{\text{SLS}})) . \quad (6)$$

This is the so-called ordinary or naive Sachs-Wolfe term (NSW), whereas the other term in (5) is called integrated Sachs-Wolfe term (ISW).

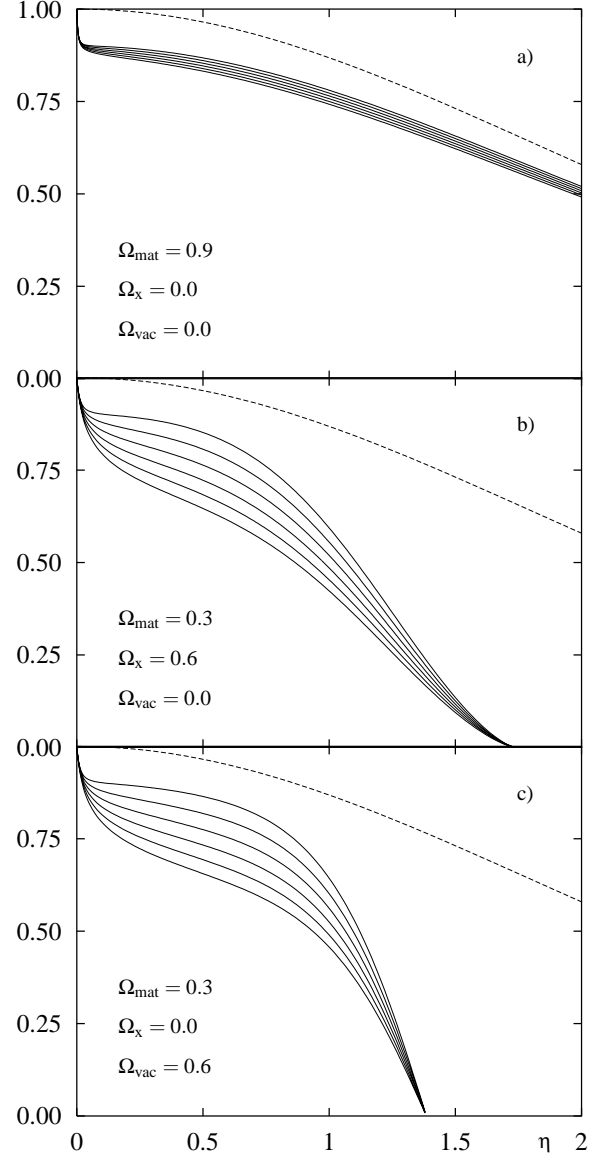


**Figure 3.** The dependence of  $f_n(\eta)/f_n(0)$  on the eigenvalue  $E_n$  is shown for  $\Omega_{\text{tot}} = 0.9$  and  $h_0 = 0.7$ . The upper full curve corresponds to  $E_n = 0$  and the lowest one to  $E_n = 5000$ . For the intermediate curves the energy is increased in steps of 1000. The dashed curve represents the result  $f_{\text{mat}}(\eta) = 5(\sinh^2\eta - 3\eta\sinh\eta + 4\cosh\eta - 4)/(\cosh\eta - 1)^3$  belonging to a pure-matter model with  $c_s = 0$  used in some related works. In a) the matter dominated case  $\Omega_{\text{mat}} = 0.9$  is shown, whereas the other two cases shown in b) and c) belong to  $\Omega_{\text{mat}} = 0.3$  and  $\Omega_x = 0.6$ ,  $\Omega_{\text{vac}} = 0.0$ , respectively,  $\Omega_x = 0.0$ ,  $\Omega_{\text{vac}} = 0.6$ .

The metric perturbation  $\Phi$  is expanded with respect to the eigenmodes

$$\Delta\psi_n(\vec{x}) = -E_n\psi_n(\vec{x}) \quad , \quad k_n := \sqrt{E_n - 1} \quad ,$$

of the considered compact orbifold, i. e.

$$\Phi(\eta, \vec{x}) = \sum_{n=1}^{\infty} f_n(\eta)\psi_n(\vec{x}) \quad ,$$

which yields for  $f_n(\eta)$  the differential equation

$$f_n''(\eta) + 3\hat{H}(1 + c_s^2)f_n'(\eta) + \{c_s^2 E_n + 2\hat{H}' + (1 + 3c_s^2)(\hat{H}^2 + 1)\}f_n(\eta) = 0 \quad , \quad (7)$$

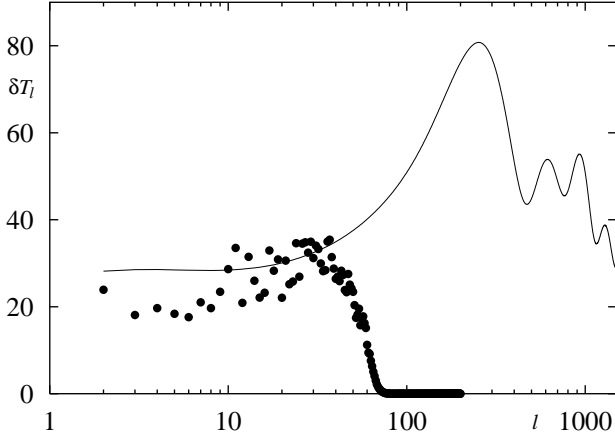


**Figure 4.** The angular power spectrum  $\delta T_l = \sqrt{l(l+1)C_l/2\pi}$  is shown for a model with  $\Omega_{\text{bar}} = 0.05$ ,  $\Omega_{\text{cdm}} = 0.25$ ,  $\Omega_{\text{x}} = 0.0$ ,  $\Omega_{\text{vac}} = 0.6$  and  $h_0 = 0.7$ . The curve is obtained from CMBFAST, whereas the dots show the result by using the discrete eigenmode spectrum.

where  $\hat{H}$  and  $c_s^2$  are determined by the background model. The initial conditions are ( $\alpha > 0$  is a normalization constant)

$$f_n(0) = \frac{\alpha}{\sqrt{k_n(k_n^2 + 1)}} \quad \text{and} \quad f_n'(0) = -\frac{f_n(0)}{8\hat{\eta}}, \quad (8)$$

which carry over to a Harrison-Zel'dovich spectrum having a spectral index  $n = 1$  and selecting only the non-decaying modes. Using the eigenmodes the perturbation is defined obeying the periodicity condition imposed by the fundamental cell.

The time dependence of  $f_n(\eta)$ , determined by the background model (3), is obtained by numerical integration of (7) and is shown in figure 3 for three different models. The first model, shown in figure 3a), is completely dominated by matter,  $\Omega_{\text{tot}} = \Omega_{\text{mat}} = 0.9$ , whereas the other two models belong to  $\Omega_{\text{mat}} = 0.3$  and  $0.6$  for  $\Omega_{\text{x}}$  and  $\Omega_{\text{vac}}$ , shown in b) and c), respectively. The latter two cases have a finite  $\eta_{\infty}$  at which the perturbation vanishes, i. e. ( $\eta \rightarrow \eta_{\infty}$ )

$$f_n(\eta) \propto (\eta_{\infty} - \eta)^{\frac{7-\sqrt{17}}{2}}$$

for the case  $\Omega_{\text{x}} > 0$  and  $\Omega_{\text{vac}} = 0$ , and

$$f_n(\eta) \propto \eta_{\infty} - \eta$$

for  $\Omega_{\text{x}} = 0$  and  $\Omega_{\text{vac}} > 0$ . Furthermore, perturbation modes with wavelength  $\lambda = \frac{2\pi}{k} > \eta_{\infty}$  will never enter the horizon in models with  $\Omega_{\text{x}} > 0$  and/or  $\Omega_{\text{vac}} > 0$ . The first decline of  $f_n(\eta)/f_n(0)$  from 1 to  $\frac{9}{10}$  for small values of  $\eta$  is due to the transition from the radiation- to the matter-dominated epoch (see, e. g. (Mukhanov et al., 1992)), which leads to the approximation (6).

With the background model (3), the time-evolution (7), and the Sachs-Wolfe formula (5), the angular power spectrum of the CMB anisotropy

$$C_l = \frac{1}{2l+1} \sum_{m=-l}^l |a_{lm}|^2$$

can be computed, where  $a_{lm}$  are the expansion coefficients of the CMB anisotropy  $\delta T$  with respect to the spherical harmonics  $Y_l^m(\theta, \phi)$ .

The angular power spectra  $\delta T_l := \sqrt{l(l+1)C_l/2\pi}$  are computed for several models. The considered compact orbifold as well as the position of the observer is the same as in (Aurich, 1999). In figure 4 the angular power spectrum  $\delta T_l$  is shown for the case

$\Omega_{\text{bar}} = 0.05$ ,  $\Omega_{\text{cdm}} = 0.25$ ,  $\Omega_{\text{x}} = 0.0$ ,  $\Omega_{\text{vac}} = 0.6$  and  $h_0 = 0.7$ . The curve is obtained from CMBFAST (Zaldarriaga and Seljak, 1999), i. e. is obtained for an infinitely extended hyperbolic universe, whereas the dots are obtained by the procedure outlined above, i. e. for a compact hyperbolic universe. Because the latter computation takes only the first 749 eigenmodes with  $k < 55$  into account, one observes at  $l \sim 40$  a decline towards zero. This is solely due to the truncation in the  $k$ -summation because the eigenmodes are only computed up to this  $k$  value. The considered modes are all above horizon at recombination, and thus the processes leading to the acoustic peak can be ignored. In the following we are only concerned with the low multipoles  $C_l$  which are affected by the non-trivial topology. These low multipoles are not affected by truncating the  $k$ -summation. The figure shows clearly the suppression in power for  $l \lesssim 10$ .

Since  $\delta T_l$  is computed for a fixed observer, i. e. it represents a ‘‘one-sky realization’’, the spectrum is not smooth like the CMBFAST spectrum. It rather shows fluctuations which an experiment would observe which necessarily measures a one-sky realization.

The lower part of the angular power spectra  $\delta T_l$ , computed for several models with a vanishing and non-vanishing  $X$ -component, are shown in figures 5 and 6, respectively. The spectra in figures 5a) and 5b) for  $\Omega_{\text{tot}} = 0.5$  and  $\Omega_{\text{tot}} = 0.8$ , respectively, show a plateau being normalized to  $30\mu\text{K}$ . At higher values of  $l$  the angular power spectra  $\delta T_l$  rise again (see figure 4) which is not shown here because our calculations do not take into account the necessary processes leading to the acoustic peak, since the modes considered here are well above the horizon at recombination. For low values of  $l$  one observes a nearly linear increase of  $\delta T_l$  which is caused by the finite size of the fundamental cell which in turn causes a cut-off in the  $k$ -spectrum. (The straight lines are drawn solely to guide the eyes.) One observes that the ‘‘bend’’ point, where the behavior turns from a linear increase to a plateau, decreases towards smaller values of  $l$  for increasing vacuum energy. If the amount of vacuum energy is replaced by the same energy contribution of an  $X$ -component one obtains quantitatively analogous angular power spectra because the behavior of  $f_n(\eta)$  shown in figure 3 is similar for vacuum energy and the  $X$ -component for  $\eta \lesssim \eta_0$ . The two models shown in figures 5c) and 5d) possess an even larger  $\Omega_{\text{tot}}$ , i. e.  $\Omega_{\text{tot}} = 0.9$  and  $\Omega_{\text{tot}} = 0.95$ , respectively. Here the suppression is much less pronounced than in the cases with  $\Omega_{\text{tot}} \lesssim 0.85$ . In the case  $\Omega_{\text{tot}} = 0.9$  the quadrupole moment is larger than the other low multipoles which is due to the large integrated Sachs-Wolfe contribution (see below). In the other case  $\Omega_{\text{tot}} = 0.95$  one observes very large fluctuations for low values of  $l$ .

For four models with an  $X$ -component the angular power spectra  $\delta T_l$  are shown in figure 6. In figure 6a) and 6b) two models with  $\Omega_{\text{tot}} = 0.9$  are shown, where in the first case the energy density is equally distributed between  $\Omega_{\text{mat}}$ ,  $\Omega_{\text{x}}$  and  $\Omega_{\text{vac}}$ , and in the second case the  $X$ -component dominates. One observes similar angular power spectra which is again explained by the similar behavior of  $f_n(\eta)$ . In both cases the multipoles with  $l \lesssim 10$  are suppressed. In figure 6c) and 6d) two models with a vanishing vacuum energy are shown for  $\Omega_{\text{tot}} = 0.9$  and  $\Omega_{\text{tot}} = 0.95$ , respectively. In the latter case the suppression of low multipoles is blurred by very large fluctuations, which occur as in figure 5d).

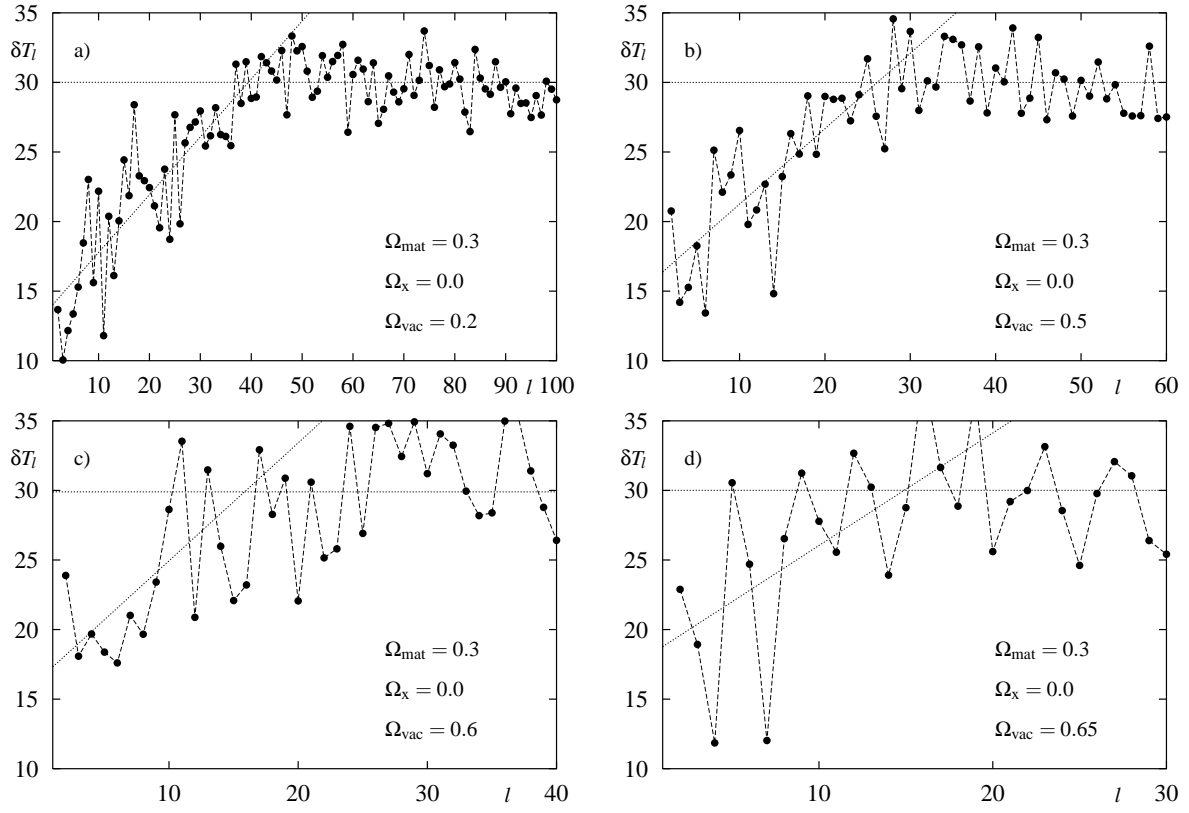


**Figure 5.** The angular power spectrum  $\delta T_l = \sqrt{l(l+1)C_l/2\pi}$  is shown in  $\mu K$  for models with a vanishing  $X$ -component.

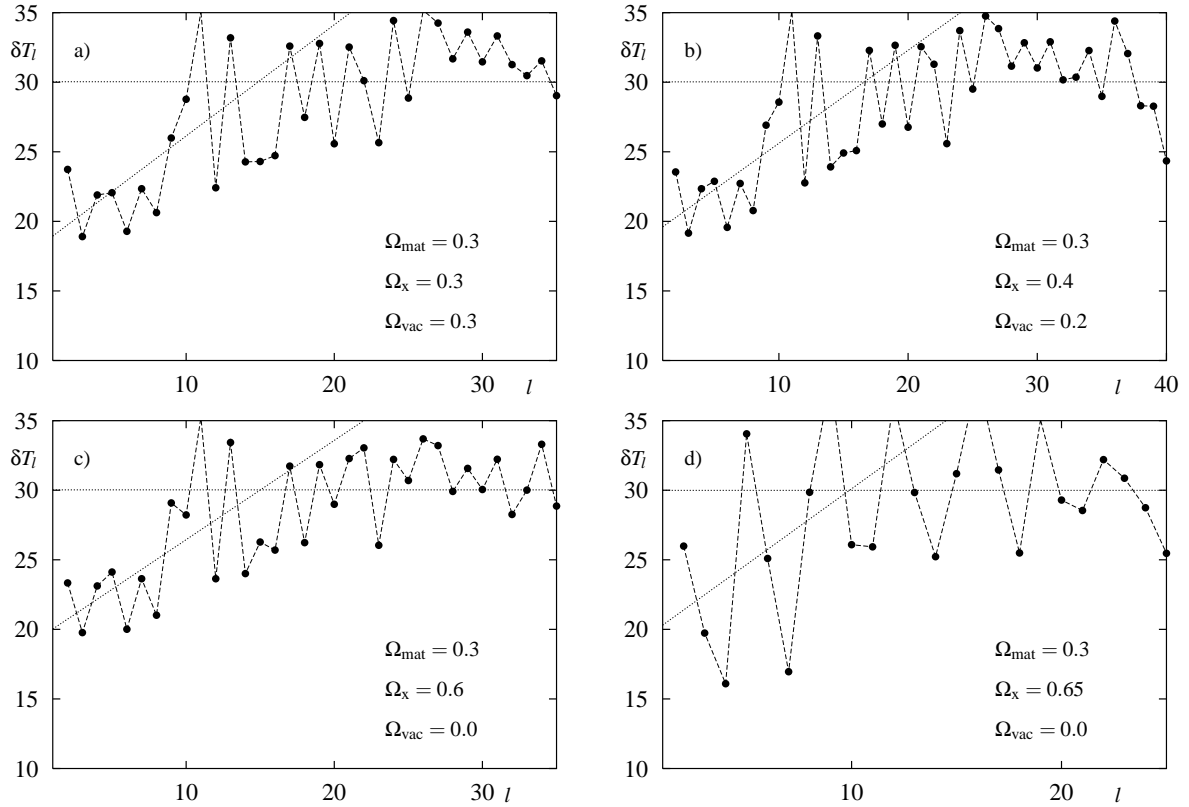


**Figure 6.** The angular power spectrum  $\delta T_l = \sqrt{l(l+1)C_l/2\pi}$  is shown in  $\mu K$  for models with an  $X$ -component.

The angular power spectrum does not go to zero at the smallest values of  $l$ . This is due to the competition of the two contributions to  $\delta T_l$ , i. e. the NSW and the ISW term in (5). As shown in figure 7 the NSW term gives a contribution which indeed vanishes for small values of  $l$  because of the cut-off in the eigenmode spectrum. But the ISW term adds an almost constant contribution which even increases towards small values of  $l$ . This interplay is responsible for the fact that  $\delta T_l$  does not fall below  $\sim 15\mu K$ , where a plateau of  $30\mu K$  is assumed. The relative contribution of the two terms is largely determined by the chosen initial conditions at  $\eta = 0$ .

The inflationary models naturally suggest isentropic initial conditions and these are imposed in the above calculations. However, imposing isocurvature initial conditions leads to a much smaller ISW contribution relative to the NSW term. This is shown in figure 7, where in figure 7a) isentropic initial conditions according to most inflationary models and in figure 7b) isocurvature initial conditions are chosen. If the observed increase in  $\delta T_l$  would be approximately linear towards zero for nearly flat models, this would imply a small ISW contribution and this would point to isocurvature initial conditions.

To summarize the results, the anomalously low quadrupole moment obtained from the COBE measurements can be taken as a first sign for a universe with a finite volume. The presented calculations demonstrate that low multipoles occur for the considered compact fundamental domain even for nearly flat, but hyperbolic, models with  $\Omega_{\text{tot}} \lesssim 0.9$ . For even larger values of  $\Omega_{\text{tot}} \simeq 0.95$  very large fluctuations occur which may also be an indication for a finite volume. Furthermore, the kind of increase of  $\delta T_l$  gives a clue to the initial conditions. Future experiments which survey the complete CMB sky like MAP and PLANCK, will have the required signal to noise ratio to reveal a possible finite universe.

## ACKNOWLEDGMENTS

We would like to thank the Rechenzentrum of the University of Karlsruhe for the access to their computers.

## REFERENCES

- Abramowitz, M. and Stegun, I. A. (1965). *Handbook of Mathematical Functions*. Dover Publications, Inc. (New York).
- Armendariz-Picon, C., Mukhanov, V., and Steinhardt, P. J. (2000a). A dynamical solution to the problem of a small cosmological constant and late-time cosmic acceleration. *astro-ph/0004134*.
- Armendariz-Picon, C., Mukhanov, V., and Steinhardt, P. J. (2000b). Essentials of k-essence. *astro-ph/0006373*.
- Atkatz, D. and Pagels, H. (1982). Origin of the universe as a quantum tunneling event. *PRD*, 25:2065–2073.
- Aurich, R. (1999). The fluctuations of the cosmic microwave background for a compact hyperbolic universe. *ApJ*, 524:497–503.
- Aurich, R. and Marklof, J. (1996). Trace formulae for three-dimensional hyperbolic lattices and application to a strongly chaotic tetrahedral billiard. *Physica D*, 118:101–129.
- Aurich, R. and Steiner, F. (1993). Statistical properties of highly excited quantum eigenstates of a strongly chaotic system. *Physica D*, 64:185–214.
- Balbi, A., Ade, P., Bock, J., Borrill, J., Boscaleri, A., de Bernardis, P., Ferreira, P. G., Hanany, S., Hristov, V. V., Jaffe, A. H., Lee, A. T., Oh, S., Pascale, E., Rabi, B., Richards, P. L., Smoot, G. F., Stompor, R., Winant, C. D., and Wu, J. H. P. (2000). Constraints on cosmological parameters from MAXIMA-1. *astro-ph/0005124*.

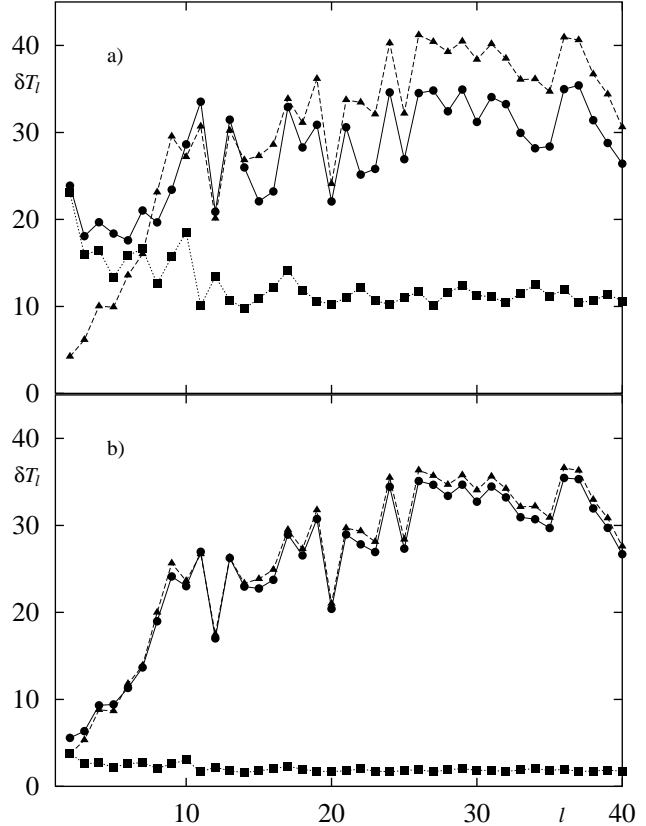


**Figure 7.** The angular power spectrum  $\delta T_l = \sqrt{l(l+1)C_l}/2\pi$  is shown in  $\mu K$  with respect to the NSW- and ISW-contributions separately for the case  $\Omega_{\text{mat}} = 0.3$ ,  $\Omega_{\text{x}} = 0.0$  and  $\Omega_{\text{vac}} = 0.6$ . In figure 7a) isentropic initial conditions are chosen, whereas in figure 7b) isocurvature initial conditions are assumed. The full circles denote the sum of both contributions, and the triangles and the squares correspond to the NSW- and ISW-contribution, respectively.

- Bond, J. R., Pogosyan, D., and Souradeep, T. (1998). Computing CMB anisotropy in compact hyperbolic spaces. *Classical Quantum Gravity*, 15:2671–2687.
- Bond, J. R., Pogosyan, D., and Souradeep, T. (2000a). CMB anisotropy in compact hyperbolic universes I: Computing correlation functions. *PRD*, 62:043005–1–20.
- Bond, J. R., Pogosyan, D., and Souradeep, T. (2000b). CMB anisotropy in compact hyperbolic universes II: COBE maps and limits. *PRD*, 62:043006–1–21.
- Caldwell, R. R., Dave, R., and Steinhardt, P. J. (1998). Cosmological imprint of an energy component with general equation of state. *PRL*, 80:1582–1585.
- Cornish, N. J. (2000). Using the acoustic peak to measure cosmological parameters. *astro-ph/0005261*.
- Cornish, N. J. and Spergel, D. (2000). A small universe after all? *PRD*, 62:087304–1–4.
- Cornish, N. J., Spergel, D., and Starkman, G. (1998). Can COBE see the shape of the universe? *PRD*, 57:5982–5996.
- de Bernardis, P., Ade, P. A. R., Bock, J. J., Bond, J. R., Borrill, J., Boscaleri, A., Coble, K., Crill, B. P., De Gasperis, G., Farese, P. C., Ferreira, P. G., Ganga, K., Giacometti, M., Hivon, E., Hristov, V. V., Iacoangeli, A., Jaffe, A. H., Lange, A. E., Martinis, L., Masi, S., Mason, P. V., Mauskopf, P. D., Melchiorri, A., Miglio, L., Montroy, T., Netterfield, C. B., Pascale, E., Piacentini, F., Pogosyan, D., Prunet, S., Rao, S., Romeo, G., Ruhl, J. E., Scaramuzzi, F., Sforza, D., and Vittorio, N. (2000). A flat universe from high-resolution maps of the cosmic microwave background radiation. *Nature*, 404(6781):955–959.

- Gabai, D., Meyerhoff, G. R., and Thurston, N. (1996). Homotopy hyperbolic 3-manifolds are hyperbolic. *MSRI preprint 1996-058*.
- Hanany, S., Ade, P., Balbi, A., Bock, J., Borrill, J., Boscaleri, A., de Bernardis, P., Ferreira, P. G., Hristov, V. V., Jaffe, A. H., Lange, A. E., Lee, A. T., Maudkopf, P. D., Netterfield, C. B., Oh, S., Pascale, E., Rabbii, B., Richards, P. L., Smoot, G. F., Stompor, R., Winant, C. D., and Wu, J. H. P. (2000). MAXIMA-1: A measurement of the cosmic microwave background anisotropy on angular scales of 10 arcminutes to 5 degrees. *astro-ph/0005123*.
- Hu, W., Fukugita, M., Zaldarriaga, M., and Tegmark, M. (2000). CMB observables and their cosmological implications. *astro-ph/0006436*.
- Hu, W. and White, M. (1996). Acoustic signatures in the cosmic microwave background. *ApJ*, 471:30–51.
- Inoue, K. T. (1999). Computation of eigenmodes on a compact hyperbolic 3-space. *Classical Quantum Gravity*, 16:3071–3094.
- Inoue, K. T., Tomita, K., and Sugiyama, N. (1999). Temperature correlations in a compact hyperbolic universe. *astro-ph/9906304*.
- Jimenez, R. (1999). Towards an accurate determination of the age of the universe. In *Proceedings of the second International Conference on Dark Matter in Astrophysics and Particle Physics, Heidelberg, Germany, 20-25 July, 1998 / edited by H.V. Klapdor-Kleingrothaus and L. Baudis. Philadelphia, PA : Institute of Physics Pub., 1999., p.170*.
- Juszkiewicz, R., Ferreira, P. G., Feldman, H. A., Jaffe, A. H., and Davis, M. (2000). Evidence for a low-density universe from relative velocities of galaxies. *Science*, 287:109–112.
- Kamionkowski, M. and Buchalter, A. (2000). The second peak: The dark-energy density and the cosmic microwave background. *astro-ph/0001045*.
- Knox, L. and Page, L. (2000). Characterizing the peak in the CMB angular power spectrum. *PRL*, 85:1366–1369.
- Lachièze-Rey, M. and Luminet, J. (1995). Cosmic topology. *Physics Report*, 254:135–214.
- Lahav, O., Lilje, P. B., Primack, J. R., and Rees, M. J. (1991). Dynamical effects of the cosmological constant. *MNRAS*, 251:128–136.
- Leggett, S. K., Ruiz, M. T., and Bergeron, P. (1998). The cool white dwarf luminosity function and the age of the galactic disk. *ApJ*, 497:294–302.
- Levin, J., Scannapieco, E., and Silk, J. (1998). Is the universe infinite or is it just really big? *PRD*, 58:103516–1–5.
- Mukhanov, V. F., Feldman, H. A., and Brandenberger, R. H. (1992). Theory of cosmological perturbations. *Physics Report*, 215:203–333.
- Peebles, P. J. E. and Ratra, B. (1988). Cosmology with a time-variable cosmological 'constant'. *ApJL*, 325:L17–L20.
- Perlmutter, S., Aldering, G., Goldhaber, G., Knop, R. A., Nugent, P., Castro, P. G., Deustua, S., Fabbro, S., Goobar, A., Groom, D. E., Hook, I. M., Kim, A. G., Kim, M. Y., Lee, J. C., Nunes, N. J., Pain, R., Pennypacker, C. R., Quimby, R., Lidman, C., Ellis, R. S., Irwin, M., McMahon, R. G., Ruiz-Lapuente, P., Walton, N., Schaefer, B., Boyle, B. J., Filippenko, A. V., Matheson, T., Fruchter, A. S., Panagia, N., Newberg, H. J. M., Couch, W. J., and The Supernova Cosmology Project (1999). Measurements of Omega and Lambda from 42 high-redshift supernovae. *ApJ*, 517:565–586.
- Primack, J. R. (2000). Cosmological parameters. *astro-ph/0007187*.
- Ratra, B. and Peebles, P. J. E. (1988). Cosmological consequences of a rolling homogeneous scalar field. *PRD*, 37:3406–3427.
- Riess, A. G., Filippenko, A. V., Challis, P., Clocchiatti, A., Diercks, A., Garnavich, P. M., Gilliland, R. L., Hogan, C. J., Jha, S., Kirshner, R. P., Leibundgut, B., Phillips, M. M., Reiss, D., Schmidt, B. P., Schommer, R. A., Smith, R. C., Spyromilio, J., Stubbs, C., Suntzeff, N. B., and Tonry, J. (1998). Observational evidence from supernovae for an accelerating universe and a cosmological constant. *AJ*, 116:1009–1038.
- Roukema, B. F. (2000). A counterexample to claimed COBE constraints on compact toroidal universe models. *astro-ph/0007140*.
- Sachs, R. K. and Wolfe, A. M. (1967). Perturbations of a cosmological model and angular variations of the microwave background. *ApJ*, 147:73–90.
- Tegmark, M. and Hamilton, A. (1997). Uncorrelated measurements of the CMB power spectrum. *astro-ph/9702019*.
- Tegmark, M. and Zaldarriaga, M. (2000). New CMB constraints on the cosmic matter budget: trouble for nucleosynthesis? *PRL*, 85:2240–2243.
- Turner, M. S. and White, M. (1997). CDM models with a smooth component. *PRD*, 56:R4439–R4443.
- Uzan, J.-P., Lehoucq, R., and Luminet, J.-P. (2000). New developments in the search for the topology of the universe. *gr-qc/0005128*.
- Wang, L., Caldwell, R. R., Ostriker, J. P., and Steinhardt, P. J. (2000). Cosmic concordance and quintessence. *ApJ*, 530:17–35.
- Weinberg, S. (2000a). The cosmological constant problems (talk given at Dark Matter 2000, February, 2000). *astro-ph/0005265*.
- Weinberg, S. (2000b). Curvature dependence of peaks in the cosmic microwave background distribution. *astro-ph/0006276*.
- Wetterich, C. (1988a). Cosmologies with variable Newton's "constant". *Nuclear Physics B*, 302:645–667.
- Wetterich, C. (1988b). Cosmology and the fate of the dilatation symmetry. *Nuclear Physics B*, 302:668–696.
- White, M. (1998). Complementary measures of the mass density and cosmological constant. *ApJ*, 506:495–501.
- White, M., Scott, D., and Pierpaoli, E. (2000). Boomerang returns unexpectedly. *astro-ph/0004385*.
- Willick, J. A. (2000). Cosmic velocities 2000: A Review. *astro-ph/0003232*.
- Winget, D. E., Hansen, C. J., Liebert, J., van Horn, H. M., Fontaine, G., Nather, R. E., Kepler, S. O., and Lamb, D. Q. (1987). An independent method for determining the age of the universe. *ApJL*, 315:L77–L81.
- Zaldarriaga, M. and Seljak, U. (1999). CMBFAST for spatially closed universes. *astro-ph/9911219*.
- Zlatev, I., Wang, L., and Steinhardt, P. J. (1999). Quintessence, cosmic coincidence, and the cosmological constant. *PRL*, 82:896–899.